Locally Conformal FDTD Modeling of MEMS-Based Antenna Sensors for Melanoma Detection

D. Caratelli, A. Yarovoy
Delft University of Technology
Delft, the Netherlands
d.caratelli@tudelft.nl

A. Massaro, R. Cingolani
Italian Institute of Technology
Arnesano, Italy
alessandro.massaro@iit.it

A. Lay-Ekuakille
University of Salento
Lecce, Italy
aime.lay.ekuakille@unisalento.it

***Abstract*—The full-wave characterization of reconfigurable antenna sensors for non-invasive detection of melanoma is presented. To this end, an enhanced locally conformal finite-difference time-domain numerical procedure, based on a suitable normalization of the electromagnetic field-related quantities, is adopted. In this way, a physical insight in wave diffraction phenomena occurring in the radar monitoring of skin cancers, as well as in the natural resonant processes responsible for the performance of the considered class of devices is achieved. This, in turn, is important in order to enhance the device reliability, so optimizing the design cycle. In this respect, a suitable micro-electro-mechanical-system-based sensor layout is proposed.**

Keywords-MEMS-based antenna sensor; locally conformal FDTD modeling; non-invasive melanoma detection

I. INTRODUCTION

Recently, microelectromechanical-system (MEMS) antennas have drawn significant interest in the design of high-performance communication devices [1], and sensors for wireless telemetry applications [2]. In particular, microsensors can be conveniently implanted in the interstitial fluid under the skin in order to monitor physiological parameters such as temperature, blood pressure, etc. As it can be readily inferred, antennas play the major role in implantable sensing devices since they directly affect the radio link with the external equipment. The design of implantable telemetry systems is very challenging due to demanding requirements in terms of reduced volume occupation, good impedance matching property, low power consumption, and biocompatibility with the human body. Furthermore, the host environment consisting of biological tissues adds significant complexity to the problem due to the high losses.

In this paper, attention is put on the analysis and design of microprobes for the detection of melanoma-related anomalies of the skin. Melanoma is a serious form of skin cancer originating in the pigment-producing cells (melanocytes). These cells become abnormal, grow uncontrollably, and aggressively invade surrounding tissues.

The detection and treatment of skin cancers have been typically addressed by means of suitable implantable microwave probes [3]. A very effective approach in the treatment of melanoma consists in the combined effect of heat and electromagnetic field radiation resulting in a localized thermal effect within the cancerous tissue to be removed. A different detection procedure has been presented in [4] where a diagnostic technique based on microwave reflectometry is considered. Suitable probes are adopted to measure the local refractive index of the skin potentially affected by melanoma-related anomalies. Finally, another approach is based on the use of implanted resonating antenna sensors, whose fundamental working frequency strongly depends on the presence of biological targets thus providing an effective means for the detection of a possible skin cancer.

In the presented study, a combined approach is proposed in order to achieve an enhanced detectability of melanomas. In particular, reconfigurable MEMS-based monopole-like sensors operating at Terahertz frequencies are used to measure, in a non-invasive way, the local variations of the permittivity due to the presence of anomalous cells on the skin surface. The design and full-wave characterization of the considered class of devices is carried out by means of a dedicated locally conformal finite-difference time-domain (FDTD) approach for accurate modeling of complex electromagnetic structures. In this way a detailed and insightful understanding of the physical processes responsible for the performance of reconfigurable antenna sensors is achieved. This in turn is very important in order to enhance the structure reliability, optimizing the design cycle. A suitable antenna layout is also proposed.

II. LOCALLY CONFORMAL FDTD TECHNIQUE

The analysis and design of complex radiating structures requires accurate electromagnetic field prediction models. One such widely used technique is the FDTD algorithm. However, in the conventional formulation proposed by Yee [5], each cell of the computational grid is implicitly supposed to be filled by a homogeneous material. For this reason, the adoption of Cartesian meshes could result in reduced numerical accuracy when structures having curved boundaries have to be modeled. In this case, locally conformal FDTD schemes [6] provide clear advantages over the use of the stair-casing approach or unstructured and stretched space lattices, potentially suffering from significant numerical dispersion and/or instability [5]. Such schemes, necessary to improve the numerical accuracy of the conventional algorithm, are based on the definition of effective material parameters suitable to describe the geometrical and electrical characteristics of the structure under analysis.

This research has been partly carried out in the framework of the *STARS* project funded by the Dutch government.

978-1-4244-9338-8/11/$26.00 ©2011 IEEE

In this section, a computationally enhanced formulation of the locally conformal FDTD scheme proposed in [6] is described. To this end, let us consider a three-dimensional domain D filled by a linear, isotropic, non dispersive material, having permittivity $\varepsilon(\boldsymbol{r})$, magnetic permeability $\mu(\boldsymbol{r})$, and electrical conductivity $\sigma(\boldsymbol{r})$. In such a domain, a dual-space, non-uniform lattice formed by a primary and secondary mesh is introduced. The primary mesh M_D is composed of space-filling hexahedrons, whose vertices are defined by the Cartesian coordinates:

$$\left\{(x_i, y_j, z_k) \mid i = 0,\ldots,N_x\,;\, j = 0,\ldots,N_y\,;\, k = 0,\ldots,N_z\right\}. \quad (1)$$

The secondary or dual mesh $\tilde{M}_D$ (see Fig. 1) is composed of the closed hexahedrons whose edges penetrate the shared faces of the primary cells and connect the relevant centroids, having coordinates $x_{i+1/2} = x_i + \Delta x_i/2$, $y_{j+1/2} = y_j + \Delta y_j/2$, $z_{k+1/2} = z_k + \Delta z_k/2$.

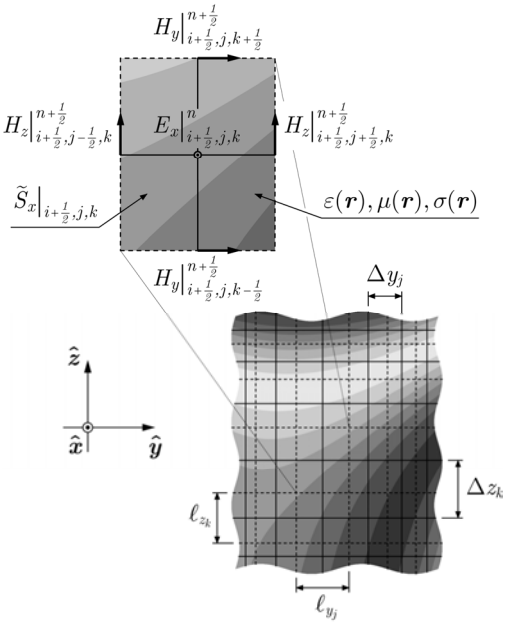

Fig. 1. Cross-sectional view of the FDTD computational grid in presence of curved boundaries between different dielectric materials.

As usual, the electric field components are defined along each edge of a primary lattice cell, whereas the magnetic field components are assumed to be located along the edges of the secondary lattice cells. In this formulation, the relationship between electric and magnetic field is given by the Maxwell's equations in integral form, using Faraday-Neumann's law and Ampere's law, respectively. In particular, the enforcement of the Ampere's law on the generic dual-mesh cell surface $\tilde{S}_x\big|_{i+1/2,j,k}$ having boundary $\partial\tilde{S}_x\big|_{i+1/2,j,k} = \tilde{C}_x\big|_{i+1/2,j,k}$ (see Fig. 1) results in the following integral equation:

$$\oint_{\tilde{C}_x\big|_{i+1/2,j,k}} \boldsymbol{H}(\boldsymbol{r},t)\cdot\boldsymbol{dl} = \iint_{\tilde{S}_x\big|_{i+1/2,j,k}} \sigma(\boldsymbol{r})E_x(\boldsymbol{r},t)dS + \\ + \frac{\partial}{\partial t}\iint_{\tilde{S}_x\big|_{i+1/2,j,k}} \varepsilon(\boldsymbol{r})E_x(\boldsymbol{r},t)dS\,, \quad (2)$$

where:

$$\oint_{\tilde{C}_x\big|_{i+1/2,j,k}} \boldsymbol{H}(\boldsymbol{r},t)\cdot\boldsymbol{dl} = \ell_{z_k}\left[H_z\left(x_{i+\frac{1}{2}}, y_{j+\frac{1}{2}}, z_k, t\right) + \right. \\ \left. - H_z\left(x_{i+\frac{1}{2}}, y_{j-\frac{1}{2}}, z_k, t\right)\right] - \ell_{y_j}\left[H_y\left(x_{i+\frac{1}{2}}, y_j, z_{k+\frac{1}{2}}, t\right) + \right. \\ \left. - H_y\left(x_{i+\frac{1}{2}}, y_j, z_{k-\frac{1}{2}}, t\right)\right] + o\left(\ell_{y_j}\right) + o\left(\ell_{z_k}\right) \quad (3)$$

as ℓ_{y_j} and ℓ_{z_k} tend to zero (see Fig. 1). Under the assumption that the spatial increments Δx_i, Δy_j, Δz_k of the computational grid are small compared to the minimum working wavelength, the infinitesimal terms of higher order appearing in (3) can be neglected. It is to be noticed that the $x-$component of the electric field is continuous along the interfaces crossing $\tilde{S}_x\big|_{i+1/2,j,k}$ so that, under the mentioned hypothesis, the following approximation can be made:

$$\iint_{\tilde{S}_x\big|_{i+1/2,j,k}} \begin{Bmatrix}\varepsilon\\ \sigma\end{Bmatrix}(\boldsymbol{r})E_x(\boldsymbol{r},t)dS \simeq \\ \simeq E_x\left(x_{i+\frac{1}{2}}, y_j, z_k, t\right)\iint_{\tilde{S}_x\big|_{i+1/2,j,k}} \begin{Bmatrix}\varepsilon\\ \sigma\end{Bmatrix}(\boldsymbol{r})dS\,. \quad (4)$$

Hence, combining the equations above yields:

$$\overline{\varepsilon}_x^{eff}\Big|_{i+\frac{1}{2},j,k}\frac{\partial}{\partial t}\mathcal{E}_x(t)\Big|_{i+\frac{1}{2},j,k} + \overline{\sigma}_x^{eff}\Big|_{i+\frac{1}{2},j,k}\mathcal{E}_x(t)\Big|_{i+\frac{1}{2},j,k} = \\ = \mathcal{H}_z(t)\Big|_{i+\frac{1}{2},j+\frac{1}{2},k} - \mathcal{H}_z(t)\Big|_{i+\frac{1}{2},j-\frac{1}{2},k} - \mathcal{H}_y(t)\Big|_{i+\frac{1}{2},j,k+\frac{1}{2}} + \\ + \mathcal{H}_y(t)\Big|_{i+\frac{1}{2},j,k-\frac{1}{2}}, \quad (5)$$

where we have introduced the normalized field quantities:

$$\mathcal{E}_x(t)\Big|_{i+\frac{1}{2},j,k} = \Delta x_i\, E_x\left(x_{i+\frac{1}{2}}, y_j, z_k, t\right), \quad (6)$$

$$\mathcal{H}_z(t)\Big|_{i+\frac{1}{2},j+\frac{1}{2},k} = \ell_{z_k}\, H_z\left(x_{i+\frac{1}{2}}, y_{j+\frac{1}{2}}, z_k, t\right), \quad (7)$$

$$\mathcal{H}_y(t)\Big|_{i+\frac{1}{2},j,k+\frac{1}{2}} = \ell_{y_j}\, H_y\left(x_{i+\frac{1}{2}}, y_j, z_{k-\frac{1}{2}}, t\right), \quad (8)$$

and the averaged effective permittivity $\overline{\varepsilon}_x^{eff}\big|_{i+1/2,j,k}$, and conductivity $\overline{\sigma}_x^{eff}\big|_{i+1/2,j,k}$, defined as follows:

$$\begin{Bmatrix}\overline{\varepsilon}\\ \overline{\sigma}\end{Bmatrix}_x^{eff}\Bigg|_{i+\frac{1}{2},j,k} = \frac{1}{\Delta x_i}\int_{z_{k-1/2}}^{z_{k+1/2}}\int_{y_{j-1/2}}^{y_{j+1/2}}\begin{Bmatrix}\varepsilon\\ \sigma\end{Bmatrix}\left(x_{i+\frac{1}{2}}, y, z\right)dydz\,. \quad (9)$$

The time derivative in (5) is then evaluated using a central-difference approximation that is second order-accurate if $E-$ and $H-$ field components are staggered in time domain [5]. This results in the following explicit time-stepping relation:

$$\mathcal{E}_x\big|^{n+1}_{i+\frac{1}{2},j,k} = \overline{\alpha}_x^{(E)}\Big|_{i+\frac{1}{2},j,k}\mathcal{E}_x\big|^{n-1}_{i+\frac{1}{2},j,k} + \overline{\beta}_x^{(E)}\Big|_{i+\frac{1}{2},j,k}(\nabla\times\boldsymbol{\mathcal{H}})_x\big|^{n+\frac{1}{2}}_{i+\frac{1}{2},j,k}\,, \quad (10)$$

where $(\nabla\times\boldsymbol{\mathcal{H}})_x\big|^{n+1/2}_{i+1/2,j,k}$ denotes the finite-difference expression of the normalized $x-$component of the magnetic field curl at the time step $n+1/2$. In (10), the information regarding the local physical and geometrical properties of the

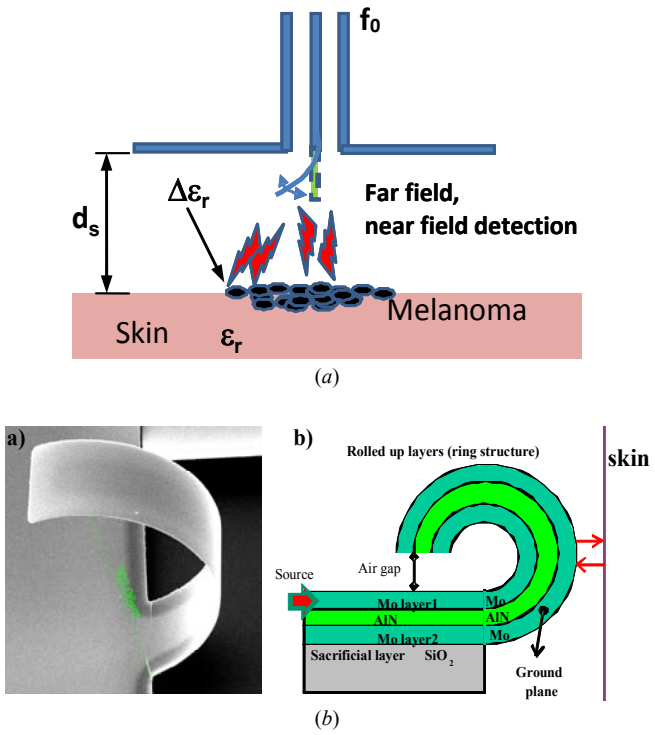

Fig. 2. MEMS-based monopole-like microsensor for non-invasive detection of melanoma-related anomalies of the skin (*a*). The antenna flair, having length $\ell_m = 1\ mm$, width $w_m = 60\ \mu m$ and thickness $t_m = 12\ \mu m$, features a curvature radius R_m which is controlled electronically by exploiting the piezoelectric property of the material forming the probe. To this end, a suitable layout consisting of an AlN film, sandwiched between Molybdenum electrodes, can be usefully adopted (*b*).

electromagnetic structure under analysis is transferred to the position-dependent coefficients $\overline{\alpha}_x^{(E)}\big|_{i+1/2,j,k}$ and $\overline{\beta}_x^{(E)}\big|_{i+1/2,j,k}$ depending on the effective material parameters. As it can be readily noticed, the computation of such coefficients can be carried out before the FDTD-method time marching starts. As a consequence, unlike in conformal techniques based on stretched space lattices, no additional correction is required in the core of the numerical algorithm. Finally, the update equations of the remaining components of the electric and magnetic field can be easily derived by permuting the spatial indices i, j, k and applying the duality principle.

III. Full-Wave Modeling of MEMS-based Monopole-like Antenna Microsensors

The growth of the melanoma results in a local variation of permittivity and electrical conductivity of the skin tissue, which can be monitored to estimate the extension of anomalous cells as function of time. The evolution of the melanoma can be analyzed by using the non-invasive microsensor system sketched in Fig. 2, consisting of a MEMS-based monopole having length $\ell_m = 1\ mm$, width $w_m = 60\ \mu m$, and thickness $t_m = 12\ \mu m$, and assumed to be at a distance $d_s = 1.2\ mm$ from the surface of the skin, modeled as a dielectric material having relative permittivity $\varepsilon_{r_{skin}} = 35.1$ and electrical conductivity $\sigma_{skin} = 3.72\ S/m$. In particular, the curvature radius R_m of the antenna flair is controlled electronically by exploiting the piezoelectric property of the material forming the probe. In this way, one can achieve an accurate scanning over a large area by properly steering the radiation beam of the antenna sensor.

The locally conformal FDTD modeling of the considered structure has been carried out on a non-uniform grid with maximum spatial increment $\Delta h_{\max} = \lambda_c/10 \simeq 25\ \mu m$, where λ_c is the working wavelength within the skin at the upper $-10dB$ cut-off frequency $f_c = 200\ GHz$ of the excitation signal, which is the Gaussian pulse described by the equation:

$$v_g(t) = V_g \exp\left[-\left(\frac{t-t_0}{t_g}\right)^2\right] u(t)\,, \tag{11}$$

where $V_g = 1\ mV$, $t_0 = 10\,t_g$, and:

$$t_g = \frac{\sqrt{\ln 10}}{\pi f_c} \simeq 2.415\ ps\,. \tag{12}$$

In (11) $u(t)$ denotes the usual Heaviside unit-step function. The source pulse is then coupled into the finite-difference equations used to update the electromagnetic field distribution within the antenna driving point. Furthermore, a ten-cell uniaxial perfectly matched layer (UPML) absorbing boundary condition for lossy media [5] has been used at the outer FDTD mesh boundary to simulate the extension of the space lattice to infinity. In doing so, a quartic polynomial grading of the UPML conductivity profile has been selected in order to have a nominal reflection error $R_{PML} \simeq e^{-16}$.

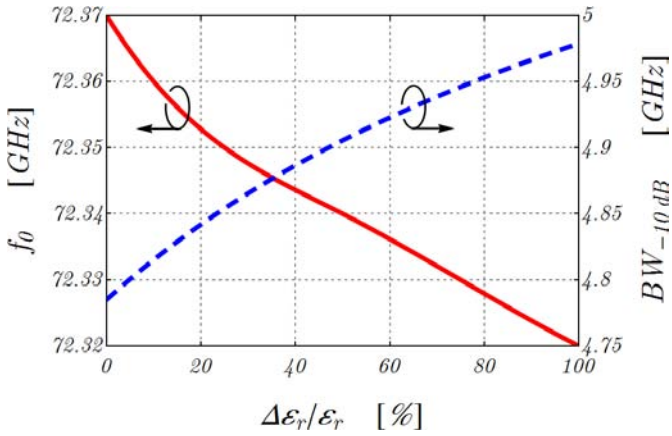

Fig. 3. Fundamental resonant frequency and bandwidth at $10dB$ return-loss level featured by the monopole-like antenna sensor as function of the relative variation $\Delta\varepsilon_r/\varepsilon_r$ of the permittivity of the skin. The probe, having curvature radius $R_m = 0.5\ mm$, is at a distance $d_s = = 1.2\ mm$ from the surface of the skin.

By using the presented electromagnetic field prediction model, a specific parameter study has been carried out in order to investigate of the probe response as a function of the relative variation $\Delta\varepsilon_r/\varepsilon_r$ of the permittivity of the skin due to the presence of the melanoma. As it can be noticed in Fig. 3, the fundamental resonant frequency f_0 of the antenna sensor having curvature radius $R_m = 0.5\ mm$ is decreasing with the relative variation of the permittivity, whereas the bandwidth at

$10dB$ return-loss level increases as $\Delta\varepsilon_r/\varepsilon_r$ becomes larger. Hence, the detection of possible anomalous areas on the skin surface can be achieved by properly tuning the central working frequency of the antenna, and by using a suitable high-sensitivity receiver to discriminate frequency points relevant to different risk levels.

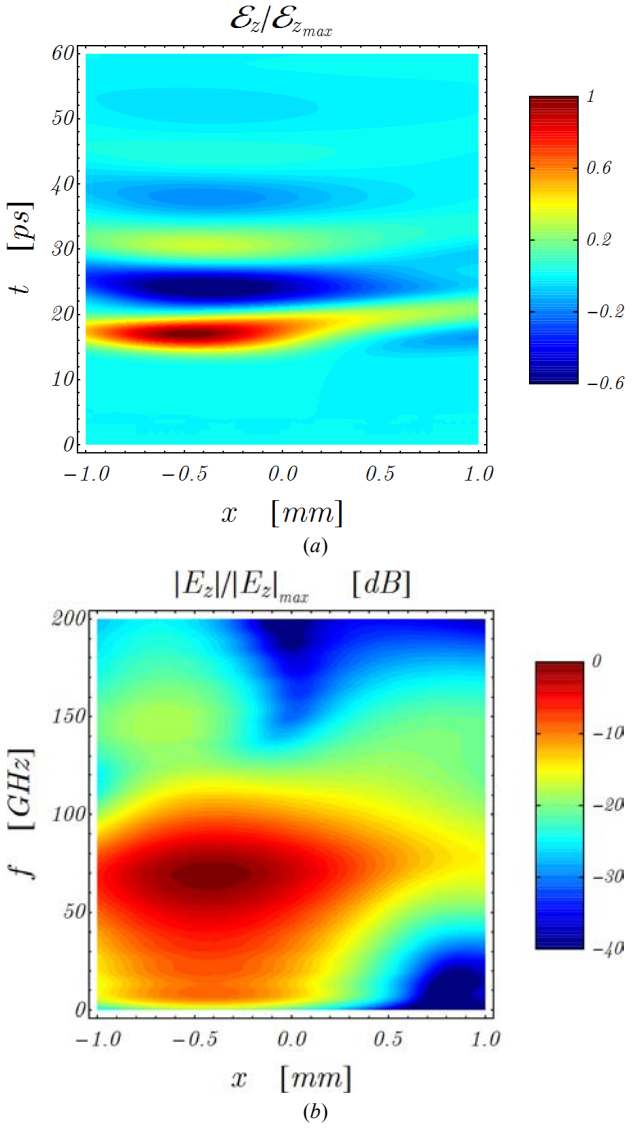

Fig. 4. Transient (*a*) and frequency-domain (*b*) behavior of the vertical component of the electric field excited by the MEMS-based monopole-like microsensor shown in Fig. 2 on the surface of the skin, modeled as a dielectric material having relative permittivity $\varepsilon_{r_{skin}} = 35.1$ and electrical conductivity $\sigma_{skin} = 3.72\ S/m$. The device is assumed to be located at $x = 0\ mm$.

The interaction of the Gaussian pulse radiated by the sensor with the target on the skin surface results in a diffracted electromagnetic field which is measured at the input terminals of the receive antenna. By changing the location of the probe and recording the response of the device as function of time (or frequency) and the sensor location, one collects the scattering data which can be processed to get a radargram of the target.

In Fig. 4, the transient and frequency-domain behavior of the vertical component of the electric field excited on the surface of the skin by the considered MEMS-based monopole-like microsensor with curvature radius $R_m = 0.5\ mm$ is shown. As it can be noticed, the radiated pulse features a reasonably small late-time ringing, which is in turn very important to prevent the masking of the target. In this way one can enhance the radiated field level, and hence increase the accuracy in the scan of anomalous areas on the skin surface. Furthermore, in order to optimize the target detectability over a large area, the radiation beam of the probe can be steered by changing the relevant curvature radius.

IV. Conclusions

The full-wave electromagnetic characterization of reconfigurable antenna sensors for the detection of melanoma-related anomalies of the skin has been presented. To this end, an enhanced locally conformal FDTD procedure has been adopted. In this way, a detailed and insightful understanding of the physical processes responsible for the performance of considered class of devices can be achieved. This in turn is very important in order to enhance the structure reliability, so optimizing the design cycle.

By using the detailed approach, the accurate time-domain modeling of MEMS-based monopole-like microsensors useful to detect local variations of the electrical properties of the skin tissue due to anomalous cells has been carried out. In this way, one can retrieve information about the growth rate of possible melanomas, which is a very important aspect regarding the monitoring of the risk. It has been numerically found that the resonant frequency of the considered sensors is significantly affected by the electrical properties of the skin. This provides an effective means to discriminate working frequency points relevant to different risk levels by using high-sensitivity receivers. A suitable antenna layout for the proposed reconfigurable detection system has been also suggested. In particular, piezoelectric electrodes controlled by a low-frequency radio signal can be used to tune the curvature radius of the probe and, hence, achieve an accurate scanning over a large area.

References

[1] C. W. Jung, M.-J. Lee, G. P. Li, and F. De Flaviis, "Reconfigurable scan-beam single-arm spiral antenna integrated with RF-MEMS switches," *IEEE Trans. Antennas Propagat.*, vol. 54, no.2, pp. 455–463, Feb. 2006.

[2] A. Massaro, I. Ingrosso, C. Giordano, M. T. Todaro, R. Cingolani, M. De Vittorio, and A. Passaseo, "Micromachining Mo/AlN/Mo piezoelectric ring resonators," *Proc. 39th European Microwave Conference*, pp. 1646–1649, 2009.

[3] L. S. Taylor, "Implantable radiators for cancer therapy by microwave hyporthermia," *Proc. IEEE*, vol. 68, no. 1, pp. 142–149, Jan. 1980.

[4] P. Mehta, K. Chand, D. Narayanswammy, D. G. Beetner, R. Zoughi, and W. V. Stoeker, "Microwave reflectometry as a novel diagnostic tool for detection of skin cancers," *IEEE Trans. Instr. Meas.*, vol. 55, no. 4, pp. 1309–1316, Aug. 2006.

[5] A. Taflove and S. C. Hagness, *Computational Electrodynamics: The Finite Difference Time Domain Method*, 3rd ed. Artech House, 2005.

[6] D. Caratelli and R. Cicchetti, "A full-wave analysis of interdigital capacitors for planar integrated circuits," *IEEE Trans. Magnetics*, vol. 39, no. 3, pp. 1598–1601, May 2003.